LIGHTWEIGHT BEAM CODEBOOK DESIGN FOR MMWAVE FULL-DUPLEX JOINT SENSING AND COMMUNICATION

Andrea Guamo-Morocho, Roberto López-Valcarce* *and Nuria González-Prelcic*†

* atlanTTic Research Center, Universidade de Vigo, Spain
†University of California San Diego, USA
emails: {aguamo,valcarce}@gts.uvigo.es, ngprelcic@ucsd.edu

ABSTRACT

The inherent self-interference (SI) can significantly compromise the performance of full-duplex (FD) joint sensing and communication (JSAC) at millimeter-Wave (mmWave) frequencies. We present a novel SI-robust design of analog beam codebooks for mmWave FD JSAC systems, with significantly lower complexity than previous approaches, while addressing the practical issue of phase shifter quantization. Numerical results show the effectiveness of the proposed method in the presence of SI, surpassing existing solutions in terms of performance.

***Index Terms*—** Full-duplex, beam codebook, mmWave, joint sensing and communication.

1. INTRODUCTION

The beamforming capabilities of massive multiple-input multiple-output (MIMO) and the wide bandwidth provided by millimeter wave (mmWave) technology are key ingredients of the emerging Joint Sensing and Communication (JSAC) paradigm [1]. Full-duplex (FD) techniques, enabling in-band simultaneous transmission and reception, represent a significant advance over traditional half-duplex (HD) in terms of not only spectral efficiency (SE) but also the ability to sense while transmitting. However, FD JSAC configurations are affected by strong self-interference (SI) coupling; thus, addressing SI is crucial to realize their full potential [1, 2, 3]. When lacking channel state information, beam alignment, *i.e.,* transmitting over training beams selected from a pre-established codebook, is typically employed to identify the optimal setting between the Base Station (BS) and the User Equipments (UEs) [4]. Developing effective codebooks is crucial to maximize system performance; while extensive research has been conducted on beam codebook design for HD systems [5, 6, 7], studies on FD systems remain scarce [8, 9]. The design in [8] for analog codebooks mitigates SI over transmit-receive beam pairs; however, it incorporates both attenuators and phase shifters, increasing complexity and power consumption. In [9] an (unquantized) phase shifter-only architecture is adopted, tackling the non-convex nature of the SI minimization problem via relaxation to transform the original problem into a sequence of convex sub-problems. This approach faces significant challenges in terms of computational complexity, which may limit its practical implementation.

We present a low-complexity design for FD JSAC analog codebooks based on phase shifters with significantly reduced execution time and complexity. Our design not only considers unquantized phase shifters but also the more practical case of finite (few bit) resolution. Numerical results show the effectiveness of our design under SI, improving the performance and computational efficiency of previous approaches.

Work funded by MCIN/AEI/10.13039/501100011033/ FEDER "A way of making Europe" under project MAYTE (PID2022-136512OB-C22) and fellowship PRE2020-096625 "ESF Investing in your future.

2. SYSTEM MODEL

Consider a mmWave FD JSAC system under two distinct scenarios as in [9], see Fig. 1. The first setting involves concurrent communication with a downlink (DL) user and an uplink (UL) user. In the second, we consider the initial access period in which the BS implements beam sweeping to discover communication users, and the transmitted signal is reflected by a target of interest and received back at the BS. In both scenarios, analog phase-shifter based arrays are assumed. The BS uses two separated, half-wavelength ($\lambda/2$) spaced uniform planar arrays (UPAs[1]) on the XZ plane, comprising $N_{\rm tx}{=}N_x^{\rm tx}N_z^{\rm tx}$ transmit and $N_{\rm rx}{=}N_x^{\rm rx}N_z^{\rm rx}$ receive antennas, resp., with $N_x^{\rm tx/rx}$, $N_z^{\rm tx/rx}$ the number of elements along the x- and z-axis. With $\otimes$ the Kronecker product, the array response vector in the direction (azimuth, elevation) $=(\phi,\theta)$ is

$$\boldsymbol{a}_{\rm BS}(\phi,\theta) = \boldsymbol{a}_x(\phi,\theta)\otimes\boldsymbol{a}_z(\theta), \quad (1)$$

$$\boldsymbol{a}_x(\phi,\theta) = [1, e^{\jmath\pi\sin\phi\cos\theta},\cdots,e^{\jmath\pi(N_x-1)\sin\phi\cos\theta}]^T, \quad (2)$$

$$\boldsymbol{a}_z(\theta) = [1, e^{\jmath\pi\sin\theta},\cdots,e^{\jmath\pi(N_z-1)\sin\theta}]^T. \quad (3)$$

The DL and UL users have uniform linear arrays (ULAs) with $N_{\rm dl}$ and $N_{\rm ul}$ antennas, resp. Their response at angle ϕ is

$$\boldsymbol{b}(\phi){=}[1, e^{\jmath\pi\sin\phi},\cdots,e^{\jmath\pi(N-1)\sin\phi}]^T,\ N{\in}\{N_{\rm dl},N_{\rm ul}\}. \quad (4)$$

In DL (resp. UL), the BS uses an analog precoder $\boldsymbol{f}\in\mathbb{C}^{N_{\rm tx}}$

[1]For concreteness only. The proposed design is not array-geometry specific.

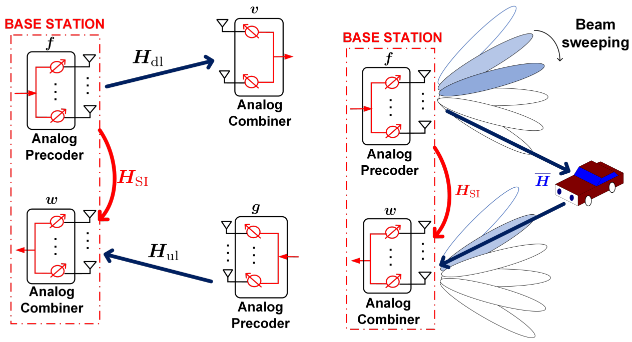

(a) Communication (b) Sensing

Fig. 1. Considered FD JSAC scenarios.

(resp. a combiner $\boldsymbol{w} \in \mathbb{C}^{N_{\mathrm{rx}}}$), and the UE applies an analog combiner $\boldsymbol{v} \in \mathbb{C}^{N_{\mathrm{dl}}}$ (resp. a precoder $\boldsymbol{g} \in \mathbb{C}^{N_{\mathrm{ul}}}$).

2.1. Communication Model

• **DL:** We adopt the widely used geometric model [10, 11] for the DL BS→UE channel matrix $\boldsymbol{H}_{\mathrm{dl}} \in \mathbb{C}^{N_{\mathrm{dl}}\times N_{\mathrm{tx}}}$:

$$\boldsymbol{H}_{\mathrm{dl}} = \sqrt{\frac{1}{L_{\mathrm{dl}}}} \sum_{l=0}^{L_{\mathrm{dl}}-1} \alpha_{\mathrm{dl},l} \boldsymbol{b}_{\mathrm{dl}}(\phi_{\mathrm{dl},l}) \boldsymbol{a}_{\mathrm{BS,tx}}^H(\phi_{\mathrm{tx},l}, \theta_{\mathrm{tx},l}), \quad (5)$$

with L_{dl}, $\alpha_{\mathrm{dl},l}$, $\phi_{\mathrm{dl},l}$ and $(\phi_{\mathrm{tx},l}, \theta_{\mathrm{tx},l})$ the number of paths, complex gain, direction of arrival (DoA) at the DL user, and azimuth/elevation of direction of departure (DoD) at the BS resp., for path l. The signal received by the DL UE is

$$y_{\mathrm{dl}} = \sqrt{P_{\mathrm{dl}}} \boldsymbol{v}^H \boldsymbol{H}_{\mathrm{dl}} \boldsymbol{f} s_{\mathrm{dl}} + \boldsymbol{v}^H \boldsymbol{n}_{\mathrm{dl}}, \quad (6)$$

with P_{dl} the DL transmit power, $s_{\mathrm{dl}}\in\mathbb{C}$ the transmitted symbol with zero mean and $\mathbb{E}\left\{|s_{\mathrm{dl}}|^2\right\} = 1/\sqrt{N_{\mathrm{tx}}}$, and $\boldsymbol{n}_{\mathrm{dl}} \sim \mathcal{CN}\left(0, \sigma_{\mathrm{dl}}^2 \boldsymbol{I}_{N_{\mathrm{dl}}}\right)$ the additive noise.

• **UL:** The UL UE→BS channel matrix $\boldsymbol{H}_{\mathrm{ul}} \in \mathbb{C}^{N_{\mathrm{rx}}\times N_{\mathrm{ul}}}$ is

$$\boldsymbol{H}_{\mathrm{ul}} = \sqrt{\frac{1}{L_{\mathrm{ul}}}} \sum_{l=0}^{L_{\mathrm{ul}}-1} \alpha_{\mathrm{ul},l} \boldsymbol{a}_{\mathrm{BS,rx}}(\phi_{\mathrm{rx},l}, \theta_{\mathrm{rx},l}) \boldsymbol{b}_{\mathrm{ul}}^H(\phi_{\mathrm{ul},l}), \quad (7)$$

with L_{ul}, $\alpha_{\mathrm{ul},l}$, $(\phi_{\mathrm{rx},l}, \theta_{\mathrm{rx},l})$, $\phi_{\mathrm{ul},l}$ analogously defined. With P_{ul} the UL transmit power, the signal received at the BS is

$$y_{\mathrm{ul}} = \sqrt{P_{\mathrm{ul}}} \boldsymbol{w}^H \boldsymbol{H}_{\mathrm{ul}} \boldsymbol{g} s_{\mathrm{ul}} + \sqrt{\rho P_{\mathrm{dl}}} \boldsymbol{w}^H \boldsymbol{H}_{\mathrm{SI}} \boldsymbol{f} s_{\mathrm{dl}} + \boldsymbol{w}^H \boldsymbol{n}_{\mathrm{ul}}, \quad (8)$$

with s_{ul} zero-mean with variance $1/\sqrt{N_{\mathrm{ul}}}$, ρ the power gain of the SI channel, and $\boldsymbol{n}_{\mathrm{ul}} \sim \mathcal{CN}(0, \sigma_{\mathrm{ul}}^2 \boldsymbol{I}_{N_{\mathrm{rx}}})$. As in [8, 9], for the SI channel $\boldsymbol{H}_{\mathrm{SI}} \in \mathbb{C}^{N_{\mathrm{rx}}\times N_{\mathrm{tx}}}$ between the TX and RX BS arrays we adopt a line-of-sight (LoS) near-field model:

$$[\boldsymbol{H}_{\mathrm{SI}}]_{pq} = \frac{\zeta}{d_{pq}} e^{-\jmath 2\pi \frac{d_{pq}}{\lambda}}, \quad \left\{ \begin{array}{lll} p & \in & \{1, \cdots, N_{\mathrm{rx}}\}, \\ q & \in & \{1, \cdots, N_{\mathrm{tx}}\}, \end{array} \right. \quad (9)$$

with d_{pq} the distance from p-th RX to q-th TX antenna, and ζ a normalizing constant so that $\|\boldsymbol{H}_{\mathrm{SI}}\|_F^2 = N_{\mathrm{tx}} N_{\mathrm{rx}}$. The sum-SE is $\mathcal{R}_{\mathrm{sum}} = \log_2(1+\mathsf{SINR}_{\mathrm{dl}}) + \log_2(1+\mathsf{SINR}_{\mathrm{ul}})$, with

$$\mathsf{SINR}_{\mathrm{dl}} = \frac{(P_{\mathrm{dl}}/N_{\mathrm{tx}}) |\boldsymbol{v}^H \boldsymbol{H}_{\mathrm{dl}} \boldsymbol{f}|^2}{\sigma_{\mathrm{dl}}^2 \|\boldsymbol{v}\|^2}, \quad (10)$$

$$\mathsf{SINR}_{\mathrm{ul}} = \frac{(P_{\mathrm{ul}}/N_{\mathrm{ul}}) |\boldsymbol{w}^H \boldsymbol{H}_{\mathrm{ul}} \boldsymbol{g}|^2}{(P_{\mathrm{dl}}\rho/N_{\mathrm{tx}}) |\boldsymbol{w}^H \boldsymbol{H}_{\mathrm{SI}} \boldsymbol{f}|^2 + \sigma_{\mathrm{ul}}^2 \|\boldsymbol{w}\|^2}. \quad (11)$$

2.2. Sensing Model

In the sensing scenario of Fig. 1(b), the BS observes echo signals for target detection during the initial access stage [9]:

$$y_{\mathrm{ul}}^{\mathrm{rf}} = \sqrt{P_{\mathrm{dl}}} \boldsymbol{w}^H \overline{\boldsymbol{H}} \boldsymbol{f} s_{\mathrm{dl}} + \sqrt{P_{\mathrm{dl}}\rho} \boldsymbol{w}^H \boldsymbol{H}_{\mathrm{SI}} \boldsymbol{f} s_{\mathrm{dl}} + \boldsymbol{w}^H \boldsymbol{n}_{\mathrm{ul}}, \quad (12)$$

with $\overline{\boldsymbol{H}} \in \mathbb{C}^{N_{\mathrm{rx}}\times N_{\mathrm{tx}}}$ the target reflection channel. The target is assumed far enough away from the BS, resulting in a monostatic setting with identical DoA and DoD (ϕ, θ):

$$\overline{\boldsymbol{H}} = \beta \boldsymbol{a}_{\mathrm{BS,rx}}(\phi, \theta) \boldsymbol{a}_{\mathrm{BS,tx}}^H(\phi, \theta), \quad (13)$$

with β the reflection coefficient with $|\beta|^2 = \frac{\lambda^2|\sigma|}{(4\pi)^3 d^4}$ [12], σ the radar cross section, and d the BS-target distance. The SINR at the BS is chosen as radar sensing performance metric:

$$\mathsf{SINR}_{\mathrm{rf}} = \frac{(P_{\mathrm{dl}}/N_{\mathrm{tx}}) |\boldsymbol{w}^H \overline{\boldsymbol{H}} \boldsymbol{f}|^2}{(P_{\mathrm{dl}}\rho/N_{\mathrm{tx}}) |\boldsymbol{w}^H \boldsymbol{H}_{\mathrm{SI}} \boldsymbol{f}|^2 + \sigma_{\mathrm{ul}}^2 \|\boldsymbol{w}\|^2}. \quad (14)$$

3. CODEBOOK DESIGN

The DL combiner and UL precoder are chosen from the columns of $\boldsymbol{B}_{\mathrm{dl}} \in \mathbb{C}^{N_{\mathrm{dl}}\times M_{\mathrm{dl}}}$ and $\boldsymbol{B}_{\mathrm{ul}} \in \mathbb{C}^{N_{\mathrm{ul}}\times M_{\mathrm{ul}}}$, resp., where M_{dl}, M_{ul} denote the number of grid points. These comprise TX and RX array responses for their respective links:

$$\boldsymbol{B}_{\mathrm{dl}} = [\, \boldsymbol{b}_{\mathrm{dl}}(\phi_{\mathrm{dl},1}) \; \boldsymbol{b}_{\mathrm{dl}}(\phi_{\mathrm{dl},2}) \; \cdots \; \boldsymbol{b}_{\mathrm{dl}}(\phi_{\mathrm{dl},M_{\mathrm{dl}}}) \,], \quad (15)$$

$$\boldsymbol{B}_{\mathrm{ul}} = [\, \boldsymbol{b}_{\mathrm{ul}}(\phi_{\mathrm{ul},1}) \; \boldsymbol{b}_{\mathrm{ul}}(\phi_{\mathrm{ul},2}) \; \cdots \; \boldsymbol{b}_{\mathrm{ul}}(\phi_{\mathrm{ul},M_{\mathrm{ul}}}) \,]. \quad (16)$$

The BS codebooks must mitigate SI while ensuring high gain at every grid point. This requires a more sophisticated approach when designing the BS codebooks, given by

$$\boldsymbol{F}_{\mathrm{BS}} = [\, \boldsymbol{f}_1 \; \boldsymbol{f}_2 \; \cdots \; \boldsymbol{f}_M \,], \; \boldsymbol{W}_{\mathrm{BS}} = [\, \boldsymbol{w}_1 \; \boldsymbol{w}_2 \; \cdots \; \boldsymbol{w}_{M'} \,], \quad (17)$$

with $\boldsymbol{f}_i \in \mathbb{C}^{N_{\mathrm{tx}}}$, $\boldsymbol{w}_i \in \mathbb{C}^{N_{\mathrm{rx}}}$, and M, M' the codebook sizes. We define the initial SI-oblivious BS codebooks, comprising TX and RX array response vectors, as

$$\boldsymbol{A}_{\mathrm{BS,tx}} = [\, \boldsymbol{a}_{\mathrm{BS,tx}}(\phi_1, \theta_1) \; \cdots \; \boldsymbol{a}_{\mathrm{BS,tx}}(\phi_M, \theta_M) \,], \quad (18)$$

$$\boldsymbol{A}_{\mathrm{BS,rx}} = [\, \boldsymbol{a}_{\mathrm{BS,rx}}(\phi_1, \theta_1) \; \cdots \; \boldsymbol{a}_{\mathrm{BS,rx}}(\phi_{M'}, \theta_{M'}) \,]. \quad (19)$$

The proposed design is captured by the following problem:

$$\min_{\boldsymbol{W}_{\mathrm{BS}}, \boldsymbol{F}_{\mathrm{BS}}} \; \|\boldsymbol{W}_{\mathrm{BS}}^H \boldsymbol{H}_{\mathrm{SI}} \boldsymbol{F}_{\mathrm{BS}}\|_F^2 \quad (20a)$$

$$\text{s. to} \quad |[\boldsymbol{A}_{\mathrm{BS,tx}}]_{:,j}^H [\boldsymbol{F}_{\mathrm{BS}}]_{:,j}| \geq \tau_j, \quad \forall j, \quad (20b)$$

$$|[\boldsymbol{A}_{\mathrm{BS,rx}}]_{:,j}^H [\boldsymbol{W}_{\mathrm{BS}}]_{:,j}| \geq \tau_j', \quad \forall j, \quad (20c)$$

$$|[\boldsymbol{F}_{\mathrm{BS}}]_{i,j}| = 1, \quad |[\boldsymbol{W}_{\mathrm{BS}}]_{i,j}| = 1, \quad \forall i, j. \quad (20d)$$

The objective in (20a) is the sum of leaked SI power for all DoA-DoD beam combinations. Parameters $\tau_j, \tau_j' > 0$ in (20b)-(20c) specify the minimum gain for each codeword: lower values enhance robustness to SI yet reduce coverage as some directions may have insufficient gain, creating a tradeoff. The unit modulus constraint of phase shifters is (20d) (the quantized phase shifter case is deferred to Sec. 4). Problem (20) was studied in [9], but the design proposed therein makes intensive use of convex solvers. Seeking lower complexity alternatives, we proceed cyclically by optimizing one analog codebook while keeping the other one fixed, and iterating:

1. Given $\boldsymbol{W}_{\text{BS}}$ and letting $\boldsymbol{M}{=}\boldsymbol{H}_{\text{SI}}^H\boldsymbol{W}_{\text{BS}}\boldsymbol{W}_{\text{BS}}^H\boldsymbol{H}_{\text{SI}}$, solve:

$$\min_{\boldsymbol{F}_{\text{BS}}} \mathsf{Tr}(\boldsymbol{F}_{\text{BS}}^H\boldsymbol{M}\boldsymbol{F}_{\text{BS}}) \tag{21a}$$

$$\text{s. to } |[\boldsymbol{A}_{\text{BS,tx}}]_{:,j}^H[\boldsymbol{F}_{\text{BS}}]_{:,j}|{\ge}\tau_j\,\forall j,\ |[\boldsymbol{F}_{\text{BS}}]_{i,j}|{=}1\,\forall i,j. \tag{21b}$$

2. Given $\boldsymbol{F}_{\text{BS}}$ and letting $\boldsymbol{M}{=}\boldsymbol{H}_{\text{SI}}\boldsymbol{F}_{\text{BS}}\boldsymbol{F}_{\text{BS}}^H\boldsymbol{H}_{\text{SI}}^H$, solve:

$$\min_{\boldsymbol{W}_{\text{BS}}} \mathsf{Tr}(\boldsymbol{W}_{\text{BS}}^H\boldsymbol{M}\boldsymbol{W}_{\text{BS}}) \tag{22a}$$

$$\text{s. to } |[\boldsymbol{A}_{\text{BS,rx}}]_{:,j}^H[\boldsymbol{W}_{\text{BS}}]_{:,j}|{\ge}\tau_j'\,\forall j,\ |[\boldsymbol{W}_{\text{BS}}]_{i,j}|{=}1\,\forall i,j. \tag{22b}$$

Problems (21) and (22) are instances of the following generic problem, with $\boldsymbol{X}\in\mathbb{C}^{N\times P}$ the optimization variable:

$$\min_{\boldsymbol{X}} \mathsf{Tr}(\boldsymbol{X}^H\boldsymbol{M}\boldsymbol{X}) \tag{23a}$$

$$\text{s. to } |\boldsymbol{e}_j^H\boldsymbol{A}_{\text{BS}}^H\boldsymbol{X}\boldsymbol{e}_j|{\ge}\eta_j\,\forall j,\ |\boldsymbol{e}_i^H\boldsymbol{X}\boldsymbol{e}_j|{=}1\,\forall i,j, \tag{23b}$$

where $\boldsymbol{M}{\succeq}\boldsymbol{0}$ and $\boldsymbol{e}_i$ is the i-th unit vector. With $\boldsymbol{x}_j{=}\boldsymbol{X}\boldsymbol{e}_j$, the objective in (23a) becomes $\sum_j \boldsymbol{x}_j^H\boldsymbol{M}\boldsymbol{x}_j$, so the problem decouples across $\{\boldsymbol{x}_j\}$. Thus, for each j we must solve

$$\min_{\boldsymbol{x}_j} \boldsymbol{x}_j^H\boldsymbol{M}\boldsymbol{x}_j \ \text{ s. to } |\boldsymbol{a}_j^H\boldsymbol{x}_j|\ge\eta_j,\ |\boldsymbol{e}_i^H\boldsymbol{x}_j|=1\,\forall i, \tag{24}$$

with $\boldsymbol{a}_j{=}\boldsymbol{A}_{\text{BS}}\boldsymbol{e}_j$. In the following we omit the column index j for brevity. Problem (24) is still non-convex; to obtain an approximate solution, we consider sequentially optimizing one particular entry $x_i{=}e^{\jmath\theta_i}$ of $\boldsymbol{x}$, while keeping the remaining ones fixed. Thus, write $\boldsymbol{x}{=}e^{\jmath\theta_i}\boldsymbol{e}_i{+}\widehat{\boldsymbol{x}}_i$, where $\widehat{\boldsymbol{x}}_i$ is obtained by zeroing the i-th component of $\boldsymbol{x}$. Then

$$\boldsymbol{x}^H\boldsymbol{M}\boldsymbol{x}{=}\boldsymbol{e}_i^H\boldsymbol{M}\boldsymbol{e}_i+2\text{Re}\{e^{\jmath\theta_i}\widehat{\boldsymbol{x}}_i^H\boldsymbol{M}\boldsymbol{e}_i\}+\widehat{\boldsymbol{x}}_i^H\boldsymbol{M}\widehat{\boldsymbol{x}}_i, \tag{25}$$

$$|\boldsymbol{a}^H\boldsymbol{x}|^2{=}|\boldsymbol{e}_i^H\boldsymbol{a}|^2+2\text{Re}\{e^{\jmath\theta_i}\widehat{\boldsymbol{x}}_i^H\boldsymbol{a}\boldsymbol{a}^H\boldsymbol{e}_i^H\}+|\widehat{\boldsymbol{x}}_i^H\boldsymbol{a}|^2. \tag{26}$$

Let $b_i{=}\boldsymbol{e}_i^H\boldsymbol{M}\widehat{\boldsymbol{x}}_i, c_i{=}\boldsymbol{e}_i^H\boldsymbol{a}\boldsymbol{a}^H\widehat{\boldsymbol{x}}_i, d_i^2{=}|\boldsymbol{e}_i^H\boldsymbol{a}|^2+|\widehat{\boldsymbol{x}}_i{}^H\boldsymbol{a}|^2$. Using (25)-(26), the problem becomes

$$\min_{\theta_i} \cos(\theta_i-\angle b_i) \quad \text{s.to} \quad \cos(\theta_i-\angle c_i)\ge\frac{\eta^2-d_i^2}{2|c_i|}, \tag{27}$$

which is feasible iff $\eta^2{\le}d_i^2{+}2|c_i|$. And since $d_i^2{+}2|c_i| = \max_\alpha |(\widehat{\boldsymbol{x}}_i+e^{\jmath\alpha}\boldsymbol{e}_i)^H\boldsymbol{a}|^2$, it follows that, if the vector $\boldsymbol{x}$ from the previous iteration was feasible for (24), then $d_i^2{+}2|c_i|^2{\ge}\eta^2$, ensuring feasibility of (27). The solution is given by

$$\theta_i{=}\begin{cases}\angle b_i{-}\pi, & \text{if } \cos(\angle c_i{-}\angle b_i)\le -s_i,\\ \displaystyle\arg\min_{\theta\in\{\theta_+,\theta_-\}} \cos\gamma_i, & \text{otherwise,}\end{cases} \tag{28}$$

where $s_i{=}\frac{\eta^2-d_i^2}{2|c_i|}$, $\gamma_i{=}\angle b_i-\theta$, $\theta_\pm{=}\angle c_i\pm\arccos(s_i)$. In this way, (24) is approached through cyclic element-wise optimization. As the objective function is non-negative and cannot increase at any iteration, convergence is guaranteed. We initialize $x_i = e^{\jmath\angle a_i}\,\forall i$, which maximizes $|\boldsymbol{x}^H\boldsymbol{a}|$ under the constraint $|x_i|{=}1,\forall i$. This results in $|\boldsymbol{w}^H\boldsymbol{a}|{=}\sum_i |a_i|$, which must not be less than η; otherwise problem (24) is unfeasible.

4. FINITE-RESOLUTION PHASE SHIFTERS

Practical phase shifters have limited resolution (say B-bit), which impacts SI mitigation capability. Each phase shifter can only synthesize the 2^B distinct phase values in $\mathcal{V}_B{=}\{1, e^{\jmath\frac{2\pi}{2^B}},\ldots,e^{\jmath\frac{2\pi}{2^B}(2^B-1)}\}$. Thus, we reformulate (20) by replacing (20d) with the constraints $[\boldsymbol{F}_{\text{BS}}]_{i,j}{\in}\mathcal{V}_B$, $[\boldsymbol{W}_{\text{BS}}]_{i,j}{\in}\mathcal{V}_B\ \forall i,j$. Then we follow an analogous cyclic approach as in Sec. 3, with (24) replaced now by

$$\min_{\boldsymbol{x}_j} \boldsymbol{x}_j^H\boldsymbol{M}\boldsymbol{x}_j \ \text{ s. to } |\boldsymbol{a}_j^H\boldsymbol{x}_j|\ge\eta_j,\ \ \boldsymbol{e}_i^H\boldsymbol{x}_j\in\mathcal{V}_B\,\forall i, \tag{29}$$

which is approached in the same way: optimize one entry of $\boldsymbol{x}_j$ at a time while keeping the others fixed, and iterate. Since $\mathcal{V}_B$ is finite, one can try out all values in $\mathcal{V}_B$ and then pick the optimum. This is repeated until convergence.

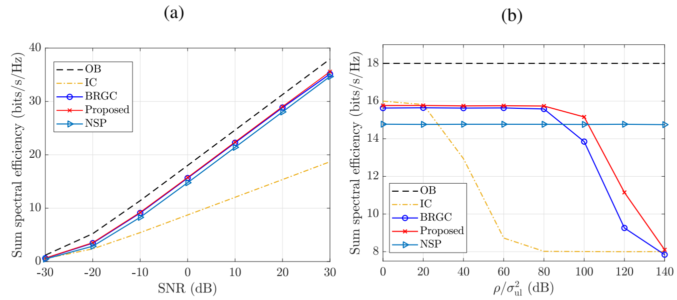

Fig. 2. Results with unquantized phase shifters. (a) $\mathcal{R}_{\text{sum}}$ vs. SNR, $\frac{\rho}{\sigma^2_{\text{ul}}}=60$ dB. (b) $\mathcal{R}_{\text{sum}}$ vs. $\frac{\rho}{\sigma^2_{\text{ul}}}$, SNR $=0$ dB.

5. NUMERICAL RESULTS

Consider an FD BS equipped with $8{\times}8$ $\lambda/2$-spaced UPAs, vertically aligned with a separation of 10λ, operating within $(\phi,\theta){\in}[-60°,60°]{\times}[-30°,30°]$. DL and UL users' 8-element ULAs operate within the azimuth range $[-60°,60°]$, with codebooks as in (15)-(16). Users are randomly deployed within the coverage area. For simplicity, a single (LoS) path is assumed for the DL and UL channels. We compare our approach with other codebook designs and benchmarks:

- **Initial Codebook (IC):** SI-oblivious codebook design based on analog beamforming, using steering vectors.
- **BRGC** [9]: A codebook based on analog beamforming with phase shifters, optimized using the CVX solver with $\epsilon_1{=}0.1$ and $\epsilon_2{=}0.3$ in [9, Eq. (12)].
- **LoneSTAR** [8]: Analog beam codebook design with both quantized phase shifters and attenuators, hence featured solely in the comparison of finite-resolution schemes.
- **Null Space Projection (NSP):** Inspired by [13], based on fully digital beamforming and used as benchmark. It maximizes the gain at each angular direction under a zero-forcing (ZF) constraint on SI.
- **Optimal Beamforming (OB):** (*Communication-Only*) Upper bound on performance, considering fully digital beamforming that uses the most dominant singular vectors of the DL and UL channels in the absence of SI.

5.1. Communication Scenario Results

We set the same SNR for DL and UL: SNR $=P_{\text{dl}}/\sigma^2_{\text{dl}} = P_{\text{ul}}/\sigma^2_{\text{ul}}$, and fix $\tau_j=0.9N_{\text{tx}}$, $\tau_j'=0.9N_{\text{rx}}\ \forall j$. As in [9], beam sweeping for DL and UL evaluates beam combinations to identify the pair maximizing received power. Both BS and

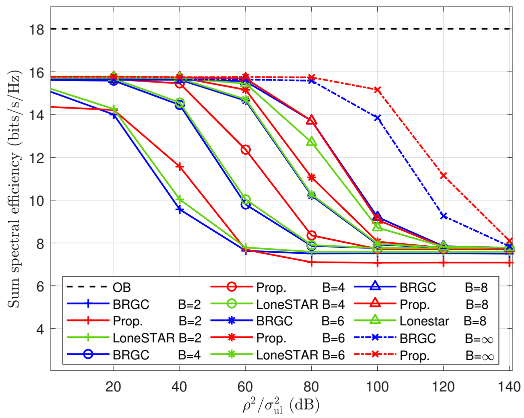

Fig. 3. $\mathcal{R}_{\rm sum}$ vs. $\frac{\rho}{\sigma_{\rm ul}^2}$. SNR=0 dB, finite-precision shifters.

users adopt a $15°$ angular grid step. Fig. 2(a) shows $\mathcal{R}_{\rm sum}$ vs. SNR, for an SI-to-noise ratio $\rho/\sigma_{\rm ul}^2 = 60$ dB, with unquantized phase shifters. IC suffers significant degradation, due to the impact of SI on the UL rate. The BRGC, NSP, and proposed designs do take SI into account, performing closer to the OB limit. While BRGC and our method perform similarly, NSP (a fully digital design) suffers a $\sim$1 bit/s/Hz loss in this setting, as the ZF constraint on SI results in fewer degrees of freedom in terms of available beamforming gain. Fig. 2(b) shows $\mathcal{R}_{\rm sum}$ vs. $\rho/\sigma_{\rm ul}^2$ at SNR $= 0$ dB. IC quickly degrades as soon as $\rho/\sigma_{\rm ul}^2 > 20$ dB, showing the need for SI-aware designs. In contrast, NSP performs consistently over the range of $\rho/\sigma_{\rm ul}^2$ values thanks to its ZF constraint enforced with a fully-digital architecture; nevertheless, its 1 bit/s/Hz loss w.r.t. analog designs is evident for moderate to high SI-to-noise ratios. Although all analog designs eventually break down under high SI, the proposed scheme is more robust than BRGC in this sense, with a $\sim$8 dB advantage; further, it is much lighter: in this setting, it ran 4.5 times faster (78% reduction in execution time) than BRGC on the same platform.

To investigate the impact of quantization, Fig. 3 shows $\mathcal{R}_{\rm sum}$ vs. $\rho/\sigma_{\rm ul}^2$ for LoneSTAR, BRGC, and the proposed design, at SNR $= 0$ dB, and for different resolutions. Whereas BRGC and our design only use phase shifters, LoneSTAR employs both phase shifters and attenuators, all quantized. Since BRGC was designed for unquantized phase shifters, we applied direct phase quantization to the analog codebooks generated by BRGC. As expected, analog codebooks degrade faster under SI with coarser quantization. The proposed design outperforms both BRGC and LoneSTAR for practical resolutions $2 \leq B \leq 6$ bits, with similar performance to BRGC for $B = 8$ bits with much less complexity. Interestingly, for sufficiently low SI levels, the effect of quantization seems to be small, *e.g.,* for $\rho/\sigma_{\rm ul}^2 \leq 40$ dB the same SE is obtained with $B = 4$ bits and with unquantized phase shifters.

5.2. Sensing Scenario Results

We let $f_c = 28$ GHz, with 300-MHz bandwidth. Transmission power is 20 dBm, thermal noise power at the RX is -89 dBm, and the SI-to-noise ratio is set to $\rho/\sigma_{\rm ul}^2 = 60$ dB. We consider a target located at 70 m from the BS, with (azimuth, elevation) $= (30°, 0°)$, and 10-m^2 radar cross-section. We compute the $\mathsf{SINR}_{\rm rf}$, see (14), by selecting the corresponding columns from the precoding and combining codebooks aligning with the same grid angle ($10°$ angular grid step). We then observe the $\mathsf{SINR}_{\rm rf}$ variation to determine the target location. Fig. 4 shows the $\mathsf{SINR}_{\rm rf}$ obtained with the BRGC and proposed codebooks. The proposed method achieves an $\mathsf{SINR}_{\rm rf}$ at the target direction of 10.6 and 2.1 dB with unquantized and 6-bit resolution phase shifters, respectively. The corresponding figures for BRGC's design are 8 and -5.5 dB.

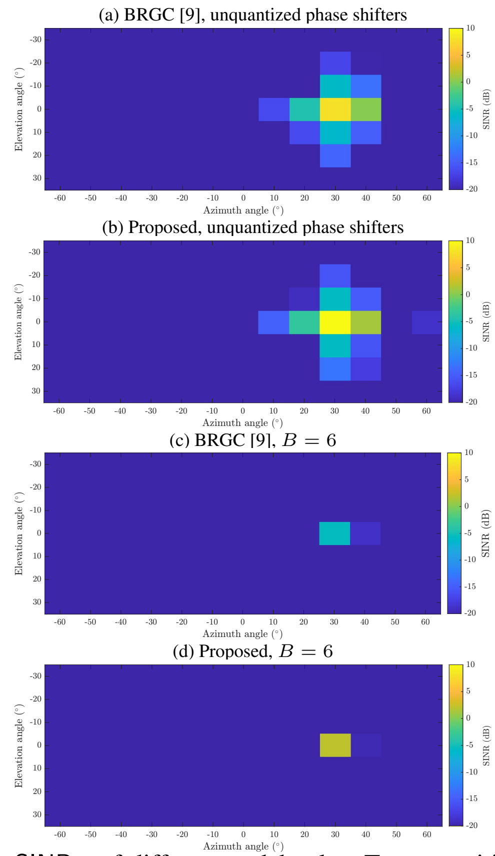

Fig. 4. $\mathsf{SINR}_{\rm rf}$ of different codebooks. Target positioned at 70 m, with azimuth angle $30°$ and elevation angle $0°$.

6. CONCLUSIONS

We have presented an analog codebook design for precoders and combiners based on phase shifters which is suitable for full-duplex operation and exhibits significant advantages over current models. It hinges on minimizing self-interference over all TX-RX beam combinations while ensuring a minimum gain level at all angular directions. A novel approach to approximately solving the corresponding problem yields significantly reduced complexity with respect to previous approaches. The proposed design enjoys enhanced robustness against interference with unquantized phase shifters and outperforms current solutions with practical phase resolutions. The results obtained highlight the potential for practical applications in both communication and sensing scenarios.

7. REFERENCES

[1] F. Liu, Y. Cui, C. Masouros, J. Xu, T. X. Han, Y. C. Eldar, and S. Buzzi, "Integrated sensing and communications: Toward dual-functional wireless networks for 6G and beyond," *IEEE J. Sel. Areas Commun.*, vol. 40, no. 6, pp. 1728–1767, 2022.

[2] N. González-Prelcic, M. F. Keskin, O. Kaltiokallio, M. Valkama, D. Dardari, X. Shen, Y. Shen, M. Bayraktar, and H. Wymeersch, "The integrated sensing and communication revolution for 6G: Vision, techniques, and applications," *Proc. IEEE*, 2024.

[3] B. Smida, G. C. Alexandropoulos, T. Riihonen, and M. A. Islam, "In-band full-duplex multiple-input multiple-output systems for simultaneous communications and sensing: Challenges, methods, and future perspectives," *IEEE Signal Process. Mag.*, vol. 41, no. 5, pp. 8–16, 2024.

[4] W. Wu, D. Liu, X. Hou, and M. Liu, "Low-complexity beam training for 5G millimeter-wave massive MIMO systems," *IEEE Trans. Veh. Technol.*, vol. 69, no. 1, pp. 361–376, 2019.

[5] M. Bayraktar, C. Rusu, N. González-Prelcic, and C. J. Zhang, "Beam codebook design for joint initial access and localization in mmwave networks," in *Proc. 56th Asilomar Conf. Signals, Syst. Comput.* IEEE, 2022, pp. 919–924.

[6] S. Mabrouki, I. Dayoub, Q. Li, and M. Berbineau, "Codebook designs for millimeter-wave communication systems in both low-and high-mobility: Achievements and challenges," *IEEE Access*, vol. 10, pp. 25786–25810, 2022.

[7] J. Tan, S. Suo, and H. Qin, "Hybrid precoding codebook design in millimetre-wave massive MIMO systems with low-resolution phase shifters," *IET Commun.*, vol. 15, no. 15, pp. 1982–1996, 2021.

[8] I. P. Roberts, S. Vishwanath, and J. G. Andrews, "LoneSTAR: Analog beamforming codebooks for full-duplex millimeter wave systems," *IEEE Trans. Wireless Commun.*, vol. 22, no. 9, pp. 5754–5769, 2023.

[9] M. Bayraktar, C. Rusu, N. González-Prelcic, and H. Chen, "Self-interference aware codebook design for full-duplex joint sensing and communication systems at mmWave," in *Proc. IEEE Int. Wkshp. Comput. Adv. Multi-Sensor Adapt. Process. (CAMSAP)*, 2023, pp. 231–235.

[10] R. W. Heath, N. González-Prelcic, S. Rangan, W. Roh, and A. M. Sayeed, "An overview of signal processing techniques for millimeter wave MIMO systems," *IEEE J. Sel. Topics Signal Process.*, vol. 10, no. 3, pp. 436–453, 2016.

[11] X. Yu, J. C. Shen, J. Zhang, and K. B. Letaief, "Alternating minimization algorithms for hybrid precoding in millimeter wave MIMO systems," *IEEE J. Sel. Topics Signal Process.*, vol. 10, no. 3, pp. 485–500, 2016.

[12] M. A. Richards, *Fundamentals of radar signal processing*, McGraw-Hill, New York, 2005.

[13] C. B. Barneto, T. Riihonen, S. D. Liyanaarachchi, M. Heino, N. González-Prelcic, and M. Valkama, "Beamformer design and optimization for joint communication and full-duplex sensing at mm-Waves," *IEEE Trans. Commun.*, vol. 70, no. 12, pp. 8298–8312, 2022.